Emission-Based Signal Timing Optimization for Isolated Intersections

Farnoush Khalighi and Eleni Christofa

Continuous growth in transportation demand in recent years has led to many traffic issues in urban areas. Among the most challenging are traffic congestion and the associated vehicular emissions. Efficient design of traffic signal control systems is a promising approach for addressing these problems. This research developed a real-time signal control system that optimizes signal timings at an undersaturated isolated intersection by minimizing total vehicular emissions. A combination of previously introduced analytical models based on traffic flow theory was used. These models estimated time spent per operating mode (i.e., time spent accelerating, decelerating, cruising, and idling) as functions of demand, vehicle arrival times, saturation flow, and signal control parameters. Information on vehicle activity was used along with the vehicle-specific power approach that provided emission rates per time spent in each operating mode to estimate the total emissions per cycle. For the evaluation of the proposed method, data from the intersection of Mesogeion and Katechaki Avenues in Athens, Greece, were used. The evaluation was performed through deterministic arrival tests under the assumption of perfect information of vehicle arrival demand and times, as well as through stochastic arrival tests in a microsimulation environment. The results reveal that the proposed emission-based optimization can substantially reduce total emissions at signalized intersections and can also lead to reduced person delay compared with the commonly used vehicle-based optimization for most cases, even under the uncertainty of stochastic arrivals.

Increases in traffic congestion caused by growth in population and in car ownership threaten mobility and quality of life in cities around the world. Traffic congestion is directly associated with reduced mobility as well as increased fuel consumption and pollutant emissions. Particularly in urban areas, motorized vehicles contribute hugely to increases in the level of air pollutants such as carbon dioxide, carbon monoxide, hydrocarbons (HC), and nitrogen oxides (NO_x). These pollutants can result in respiratory, nervous, and cardiovascular diseases (*1*). A major challenge for crowded cities is to improve air quality while maintaining efficient and reliable traffic and transit operations. Traffic signal systems that are widely available in urban areas can be used to make traffic operations more efficient while reducing vehicle pollutant emissions.

Although signal control systems traditionally have been designed only to reduce delay (*2, 3*), in recent years the study of the impacts of such strategies on vehicle emissions has attracted a lot of attention (*4–7*). Extensive literature exists on the effects of traffic signal control strategies on emissions. Studies have been performed with field measurements (*4, 7–10*), simulation tests (*11–15*), and analytical models (*16, 17*). Field studies are more accurate than other methods because they can measure the actual exhaust emissions during real-world operations. However, their implementation is costly and they are not always feasible. Traffic simulation studies combine the use of simulation tools for obtaining vehicle activity with emission models for estimating modal or instantaneous vehicle emissions. Although most simulation tests can capture second-by-second changes of speed and acceleration levels, they are time-consuming, and the results cannot be easily extended to other cases. In addition, a recent study has identified that second-by-second microsimulation trajectories are not appropriate for accurate emission estimation, even for well-calibrated microsimulation models (*18*). Hence, there is a need for analytical models that have fewer parameters and that consequently lower computation times for emission estimation.

Existing analytical models usually estimate emissions from average speed. However, average speed cannot capture the effects of instantaneous speed changes on emissions. Studies show that vehicle movements with the same average speed and different speed changes and acceleration levels produce different emission levels. Nonsmooth traffic operations and stop-and-go vehicle movements are the main causes of high emission levels at urban intersections (*8, 11, 19*) because they result in more time spent in acceleration, which in turn results in the vehicle's engine operating at higher power. Particularly, in acceleration modes that occur at higher speeds, the engine's power substantially increases, affecting the level of vehicle emissions (*20–22*). In a few recent studies (*16, 17*), analytical models were developed to describe the effect of traffic on the time spent in each vehicle operation mode (i.e., acceleration, deceleration, idling, and cruising) and then to incorporate emission factors per operating mode to obtain emission levels at signalized intersections.

A thorough review of the literature shows that although some models for estimation of modal emissions have been developed, there is no real-time signal timing optimization algorithm for minimizing emissions that have been estimated with these models. This study develops a real-time signal control strategy to minimize emissions at an isolated intersection that operates in undersaturated traffic conditions. The proposed emission-based signal control optimization can help transportation agencies use traffic signals to minimize emissions in critically polluted areas.

The rest of the paper is organized as follows. First, the analytical models used to estimate emissions for both autos and transit vehicles are described, along with the mathematical model used to minimize total emissions. Next, a description of the test site used to assess the performance of the proposed system is presented. The results from the deterministic and stochastic arrival tests performed

F. Khalighi, 139 Marston Hall, and E. Christofa, 216 Marston Hall, Department of Civil and Environmental Engineering, University of Massachusetts, Amherst, 130 Natural Resources Road, Amherst, MA 01003. Corresponding author: E. Christofa, christofa@ecs.umass.edu.

Transportation Research Record: Journal of the Transportation Research Board, No. 2487, Transportation Research Board, Washington, D.C., 2015, pp. 1–14.
DOI: 10.3141/2487-01

with the emission-based signal timing optimization are compared with the commonly used vehicle-based signal control and a person-based optimization strategy developed by Christofa et al. (*23, 24*). Finally, the findings of the study are summarized and suggestions for future work are made.

METHODOLOGY

This paper develops an emission-based real-time signal control system whose mathematical model and emission estimation model formulations are based on previous research. Christofa et al. developed a person-based signal control system that provides priority to transit vehicles by accounting for their higher passenger occupancy (*23, 24*). The proposed system focuses on minimization of total emissions from both autos and transit vehicles. Vehicle emissions vary significantly by operating mode. The amount of emissions produced per second spent in acceleration is much higher than that in other modes. Hence, for estimating emissions, time spent in the various modes is predicted with a model incorporating a model developed by Shabihkhani and Gonzales (*16*) and a model developed by Christofa et al. (*24*). This information is then used along with modal emission rates for estimating total emission levels.

Calculation of emission rates is based on the vehicle-specific power (VSP) mode (*21, 25*). VSP is an indicator of engine power demand (i.e., a higher VSP value is correlated with higher fuel consumption and emissions). Emission estimation approaches that use VSP categorize vehicle operating modes into several VSP bins that are defined according to vehicle speed and acceleration rates and provide emission rates for each VSP bin (*20, 21*).

The proposed real-time emission-based strategy for signal timing optimization is tested through both deterministic and stochastic arrival tests at an isolated intersection. Deterministic arrival tests are performed under the assumption of perfect information on all inputs; stochastic arrival tests are performed with microsimulation software where perfect information is not available in real time and estimates of input values are used instead. The vehicle emission and person delay estimates obtained in the deterministic arrival tests scenario are compared with those obtained from the simulation tests, as well as with results obtained when the previously published person-based optimization model is implemented (*23, 24*). For calculating vehicle operating times, cruising speed and acceleration and deceleration rates are assumed to be constant. It is also assumed that auto and transit vehicles travel in the same lanes. In addition, it is assumed that the vehicle arrival rates are deterministic and that the capacity for each approach at the intersection is fixed and known. Signal cycle length, phase sequence, and yellow times are constant in this signal control strategy, and only phase splits are optimized for every cycle. Additionally, certain upper and lower bounds are assumed for the green times of each phase, which guarantees that no phase is skipped and guarantees minimum green times for each lane group.

Figure 1 is a queuing diagram for an intersection in undersaturated traffic conditions. This diagram can be used to estimate the number of stops as well as the time spent in idling for both autos and transit vehicles. As the figure shows, each lane group has a constant vehicle arrival rate, which is denoted by q_j vps. A lane group is defined as one or more adjacent lanes at each intersection approach that can be served by the same phases (*26*).

As shown in Figure 1, certain components of each cycle are defined as follows to simplify the formulation of the analytical model:

$$R_j^{(1)}(g_{i,T}) = \sum_{i=1}^{k_j-1} g_{i,T} + \sum_{i=1}^{k_j-1} y_i \tag{1}$$

$$G_j^e(g_{i,T}) = \sum_{i=k_j}^{l_j} g_{i,T} + \sum_{i=k_j}^{l_j-1} y_i \tag{2}$$

$$R_j^{(2)}(g_{i,T}) = \sum_{i=l_j+1}^{I} g_{i,T} + \sum_{i=l_j}^{I} y_i \tag{3}$$

The generalized formulation of the mathematical program that minimizes emissions for all vehicles at one intersection for a signal cycle T is as follows:

$$\min \sum_{a=1}^{A_T} \sum_m e_m^a t_{a,m} + \sum_{b=1}^{B_T} \sum_m e_m^b t_{b,m} \qquad \forall m \in \{\text{id, cr, acc, dec}\} \tag{4}$$

$$g_{i\min} \le g_{i,T} \le g_{i\max} \qquad \forall i \tag{5}$$

$$\sum_{i=k_j}^{l_j} g_{i,T} + \sum_{i=k_j}^{l_j-1} y_i \ge g_{j\min} \qquad \forall j \tag{6}$$

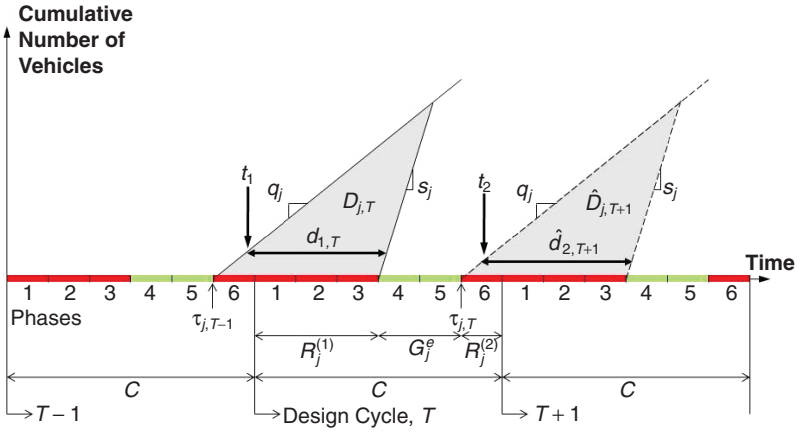

FIGURE 1 Queuing diagram for lane group *j* for undersaturated conditions (*24*).

$$\sum_{i=1}^{I} g_{i,T} + L = C \tag{7}$$

where

A_T = total number of autos that are considered in the optimization of cycle T,
B_T = total number of transit vehicles that are considered in the optimization of cycle T,
e_m^a = emission rate of auto a during operating mode m (g/s),
e_m^b = emission rate of transit vehicle b during operating mode m (g/s),
$t_{a,m}$ = time spent in mode m by auto a (s),
$t_{b,m}$ = time spent in mode m by transit vehicle b (s),
id = idling mode,
cr = cruising mode,
acc = acceleration mode,
dec = deceleration mode,
$g_{i,T}$ = green time allocated to phase i in cycle T (s),
$g_{i\,\min/\max}$ = minimum or maximum green time of phase i (s),
k_j,l_j = first or last phase in a cycle that can serve lane group j,
y_i = yellow time of phase i (s),
$g_{j\,\min}$ = minimum green time of lane group j (s),
I = total number of phases in a cycle,
L = total lost time per cycle (s), and
C = cycle length (s).

The next sections explain the models used to estimate vehicle emissions. A detailed description of the person-based signal control strategy is available elsewhere (*24*).

Time Spent in Various Vehicle Operating Modes

Automobiles

Time Spent Accelerating or Decelerating Because vehicles spend some time in the deceleration and acceleration modes before and after each stop, estimating the total number of vehicle stops at the intersection is the first step in estimating time spent in these modes (*16*). In undersaturated conditions, the focus of this paper, vehicles stop at most once upstream of the intersection, so the total number of vehicle stops is equal to the number of vehicles that cannot pass through the intersection without stopping. Equation 8, adopted from the work of Shabihkhani and Gonzales (*16*), calculates automobile stops for a single cycle *T*. To account for the effects of signal timing optimization of design cycle, *T,* on the next cycle, $T + 1$, the sum of auto emissions for both cycles is included in the objective function as was done by Christofa et al. for total person delay (*24*). In this case, the number of stops during both cycles T and $T + 1$ is estimated as follows:

$$N_{S,T} = \sum_{j=1}^{J} \frac{q_j}{1 - \frac{q_j}{s_j}} \left(R_j^{(2)}\left(g_{i,T-1}\right) + R_j^{(1)}\left(g_{i,T}\right) \right) \tag{8}$$

$$N_{S,T+1} = \sum_{j=1}^{J} \frac{q_j}{1 - \frac{q_j}{s_j}} \left(R_j^{(2)}\left(g_{i,T}\right) + R_j^{(1)}\left(g_{i\,\text{next}}\right) \right) \tag{9}$$

where $g_{i\,\text{next}}$ is the assumed green times for cycle $T + 1$, which in this study are set to the fixed-time optimal green times provided by TRANSYT-7F (*27*). The assumed values for $g_{i\,\text{next}}$ do not affect the results considerably because the values will be updated during the optimization of cycle $T + 1$. If it is assumed that autos decelerate or accelerate at a constant rate, the total time spent in these modes during cycle *T,* $t_{a,\text{acc/dec},T}$, and $T + 1$, $t_{a,\text{acc/dec},T+1}$, can be estimated with Equations 10 and 11.

$$t_{a,\text{acc/dec},T} = \frac{v_{a,\text{cr}}}{\alpha_{a,\text{acc/dec}}} \left[\sum_{j=1}^{J} \frac{q_j}{1 - \frac{q_j}{s_j}} \left(R_j^{(2)}\left(g_{i,T-1}\right) + R_j^{(1)}\left(g_{i,T}\right) \right) \right] \tag{10}$$

$$t_{a,\text{acc/dec},T+1} = \frac{v_{a,\text{cr}}}{\alpha_{a,\text{acc/dec}}} \left[\sum_{j=1}^{J} \frac{q_j}{1 - \frac{q_j}{s_j}} \left(R_j^{(2)}\left(g_{i,T}\right) + R_j^{(1)}\left(g_{i\,\text{next}}\right) \right) \right] \tag{11}$$

where

$v_{a,\text{cr}}$ = average cruising speed of approaching autos (m/s),
$\alpha_{a,\text{acc/dec}}$ = average acceleration or deceleration rate of autos (m/s^2),
s_j = saturation flow of lane group j (vps), and
J = number of lane groups at the intersection.

Time Spent Idling When approaching an intersection, an auto traveling at cruising speed stops at the back of the queue; when the signal turns green and the lane group's queue dissipates, autos move forward at cruising speed. Examples of such trajectories are shown in Figure 2. The time–space diagram assumes that traffic conditions can be represented by a triangular fundamental diagram, like the one in Figure 2*a.* However, vehicles cannot instantaneously stop or reach cruising speed. In reality, they travel some time in deceleration and acceleration modes, as shown in Figure 2*c.* As the figure indicates, some of the time considered to be idling or cruising is actually deceleration or acceleration mode. Hence, half the required time for deceleration and acceleration is subtracted from the idling mode and half is subtracted from the cruising mode.

Queuing diagrams like the one illustrated in Figure 1 allow delays to be estimated for both autos and transit vehicles. Because the *y*-axis of this graph represents the cumulative number of arriving and departing vehicles from the intersection, the areas $D_{j,T}$ and $\hat{D}_{j,T+1}$ represent the total auto delay at the intersection for cycles T and $T+1$, respectively. However, half the total deceleration and acceleration time should be subtracted from the total auto delay (i.e., idling time) for cycle *T,* $D_{j,T}$ and the total auto delay for cycle $T + 1$, $\hat{D}_{j,T+1}$. Hence, for all autos that stop, the time spent idling in cycles T and $T + 1$ can be calculated as follows:

$$t_{a,\text{id},T} = \frac{1}{2} \sum_{j=1}^{J} \left[\frac{q_j}{1 - \frac{q_j}{s_j}} \left(R_j^{(2)}\left(g_{i,T-1}\right) + R_j^{(1)}\left(g_{i,T}\right) \right)^2 \right] - \left(\frac{t_{a,\text{acc},T} + t_{a,\text{dec},T}}{2} \right) \tag{12}$$

$$t_{a,\text{id},T+1} = \frac{1}{2} \sum_{j=1}^{J} \left[\frac{q_j}{1 - \frac{q_j}{s_j}} \left(R_j^{(2)}\left(g_{i,T}\right) + R_j^{(1)}\left(g_{i\,\text{next}}\right) \right)^2 \right] - \left(\frac{t_{a,\text{acc},T+1} + t_{a,\text{dec},T+1}}{2} \right) \tag{13}$$

Time Spent Cruising For the estimation of cruising time, one must consider certain lengths for sections both upstream and downstream of the intersection to ensure that vehicles that stop experience a full operating cycle. This adjustment is made because not all vehicles

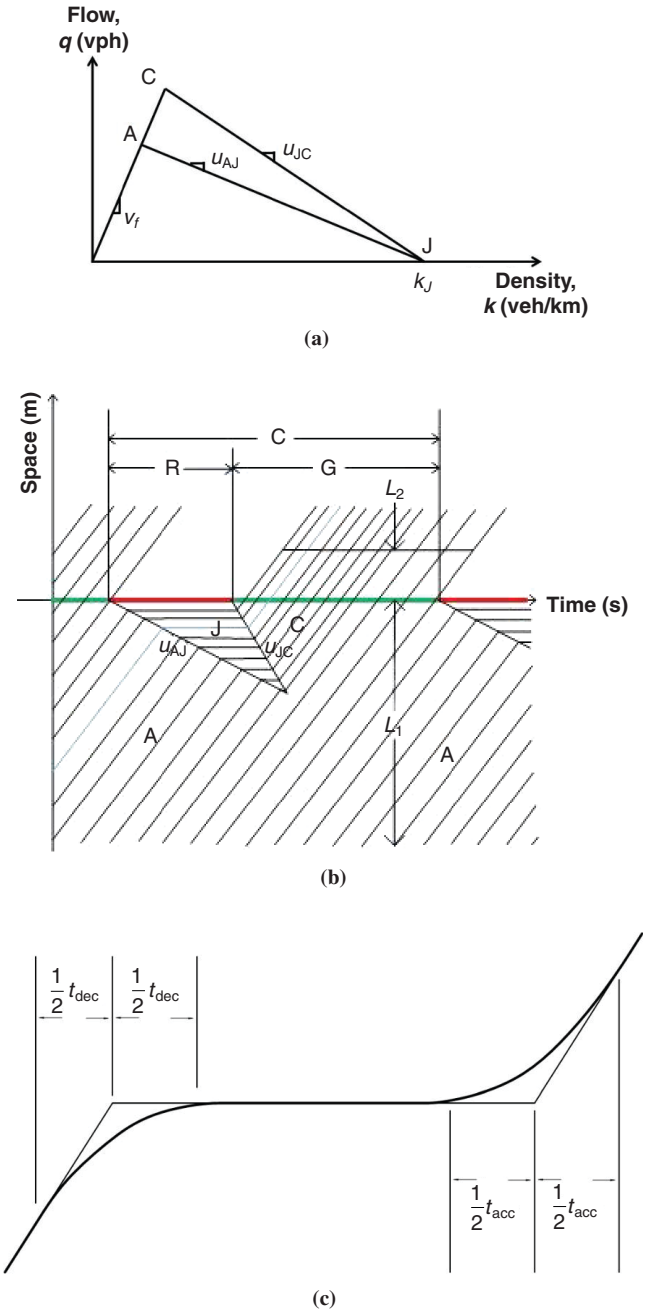

FIGURE 2 Intersection approach in undersaturated conditions: (*a*) fundamental diagram, (*b*) time–space diagram, and (*c*) acceleration–deceleration cycle for single stop.

experience a full operating cycle. Autos that arrive during the green phase after the clearance of their lane group's queue can pass the intersection without stopping and travel the whole link distance in cruising mode. Distances upstream and downstream of the intersection are defined as L_1 and L_2, respectively, and are shown in Figure 2*b*. L_1 and L_2 are long enough to ensure a complete operating cycle (i.e., cruising, decelerating, idling, accelerating, and again cruising) for vehicles that have to stop at the intersection. The cruising time of vehicles during cycles T and $T+1$ is estimated with Equations 14 through 19. Equations 14 and 17 calculate time spent in cruising mode for autos that have to stop in cycles T and $T+1$, which are denoted $t^{(1)}_{a,\mathrm{cr},T}$ and $t^{(1)}_{a,\mathrm{cr},T+1}$, respectively. Equations 15 and 18 calculate time spent in cruising mode for vehicles that do not have to stop in cycles T and $T+1$, which are denoted $t^{(2)}_{a,\mathrm{cr},T}$ and $t^{(2)}_{a,\mathrm{cr},T+1}$, respectively. Then total time spent in cruising mode in cycles T and $T+1$, $t_{a,\mathrm{cr},T}$ and $t_{a,\mathrm{cr},T+1}$, is calculated with Equations 16 and 19, respectively:

$$t^{(1)}_{a,\mathrm{cr},T}=\sum_{j=1}^{J}\left[\frac{q_j}{1-\frac{q_j}{s_j}}\left(R^{(2)}_j\left(g_{i,T-1}\right)+R^{(1)}_j\left(g_{i,T}\right)\right)\left(\frac{L_1+L_2}{v_{a,\mathrm{cr}}}\right)\right]-\left(\frac{t_{a,\mathrm{acc},T}+t_{a,\mathrm{dec},T}}{2}\right) \tag{14}$$

$$t^{(2)}_{a,\mathrm{cr},T}=\frac{L_1+L_2}{v_{a,\mathrm{cr}}}\left[q_jC-\frac{q_j}{1-\frac{q_j}{s_j}}\left[R^{(2)}_j\left(g_{i,T-1}\right)+R^{(1)}_j\left(g_{i,T}\right)\right]\right] \tag{15}$$

$$t_{a,\mathrm{cr},T}=t^{(1)}_{a,\mathrm{cr},T}+t^{(2)}_{a,\mathrm{cr},T} \tag{16}$$

$$t^{(1)}_{a,\mathrm{cr},T+1}=\sum_{j=1}^{J}\left[\frac{q_j}{1-\frac{q_j}{s_j}}\left(R^{(2)}_j\left(g_{i,T}\right)+R^{(1)}_j\left(g_{i\,\mathrm{next}}\right)\right)\left(\frac{L_1+L_2}{v_{a,\mathrm{cr}}}\right)\right]-\left(\frac{t_{a,\mathrm{acc},T+1}+t_{a,\mathrm{dec},T+1}}{2}\right) \tag{17}$$

$$t^{(2)}_{a,\mathrm{cr},T+1}=\sum_{j=1}^{J}\frac{L_1+L_2}{v_{a,\mathrm{cr}}}\left[q_jC-\frac{q_j}{1-\frac{q_j}{s_j}}\left[R^{(2)}_j\left(g_{i,T}\right)+R^{(1)}_j\left(g_{i\,\mathrm{next}}\right)\right]\right] \tag{18}$$

$$t_{a,\mathrm{cr},T+1}=t^{(1)}_{a,\mathrm{cr},T+1}+t^{(2)}_{a,\mathrm{cr},T+1} \tag{19}$$

The total auto emissions component of the objective function is as follows:

$$\sum_{a=1}^{A_T}\sum_{m}e^a_m t_{a,m}=e^a_{\mathrm{id}}t_{a,\mathrm{id},T}+e^a_{\mathrm{cr}}t_{a,\mathrm{cr},T}+e^a_{\mathrm{acc}}t_{a,\mathrm{acc},T}+e^a_{\mathrm{dec}}t_{a,\mathrm{dec},T}+e^a_{\mathrm{id}}t_{a,\mathrm{id},T+1}+e^a_{\mathrm{cr}}t_{a,\mathrm{cr},T+1}+e^a_{\mathrm{acc}}t_{a,\mathrm{acc},T+1}+e^a_{\mathrm{dec}}t_{a,\mathrm{dec},T+1} \tag{20}$$

Transit Vehicles

The time estimation for all operating modes of transit vehicles except idling is similar to that for autos. For the estimation of transit delay (i.e., idling time) and emissions, only transit vehicles that are served or arrive during the design cycle T are considered. Transit vehicles that arrive in cycle $T+1$ are not taken into account for the optimization of cycle T because their arrival time information is not available for optimizing cycle T. Transit vehicles that arrive during cycle $T+1$ are considered in the optimization of the next cycle.

Assuming that transit vehicles decelerate or accelerate at a constant rate, the total time spent on these modes during cycle T, $t_{b,\mathrm{acc/dec},T}$, can be estimated similarly to Equation 10, as follows:

$$t_{b,\mathrm{acc/dec},T}=\frac{v_{b,\mathrm{cr}}}{\alpha_{b,\mathrm{acc/dec}}} \tag{21}$$

where

$t_{b,\mathrm{acc/dec},T}$ = time spent in acceleration or deceleration by transit vehicle b during cycle T (s),

$v_{b,\mathrm{cr}}$ = cruising speed for transit vehicle b (m/s), and
$\alpha_{b,\mathrm{acc/dec}}$ = average acceleration or deceleration rate of transit vehicle b (m/s^2).

The idling time of a transit vehicle, b, depends on its arrival time at the back of this lane group's queue, t_b, relative to the end of the last phases that can serve its lane group in cycles $T-1$ and T, which are denoted $\tau_{j,T-1}$ and $\tau_{j,T}$, respectively (Figure 1).

$$\tau_{j,T-1} = (T-2)C + R_j^{(1)}(g_{i,T-1}) + G_j^e(g_{i,T-1}) \tag{22}$$

$$\tau_{j,T} = (T-1)C + R_j^{(1)}(g_{i,T}) + G_j^e(g_{i,T}) \tag{23}$$

Figure 1 shows examples of two transit vehicles that arrive at times t_1 and t_2 and their corresponding delays, $d_{1,T}$ and $\hat{d}_{2,T+1}$, that are used to estimate bus idling time. Transit vehicles are categorized into three groups according to their arrival time:

- Transit vehicles that arrive before the end of their green phase in cycle T and before the queue has dissipated. This time interval is denoted α. $d_{1,T}$ in Figure 1 represents the delay for a transit vehicle of this group.
- Transit vehicles that arrive before the end of their green phase in cycle T but after the queue has dissipated. The time interval of this group is denoted β. These vehicles experience no delay and pass through the intersection without stopping.
- Transit vehicles that arrive after the end of their green phase in cycle T. This time interval is denoted γ. $\hat{d}_{2,T+1}$ in Figure 1 represents the delay for a transit vehicle in this group.

The idling time for transit vehicles in these groups, accounting for part of the delay being allocated in acceleration or deceleration mode, is calculated with Equations 24 through 26:

$$t_{b,\mathrm{id},T}^{\alpha} = (T-1)C + R_j^{(1)}(g_{i,T}) + \frac{q_j}{s_j}(t_b - \tau_{j,T-1}) - t_b - \left(\frac{t_{b,\mathrm{acc},T} + t_{b,\mathrm{dec},T}}{2}\right) \tag{24}$$

$$t_{b,\mathrm{id},T}^{\beta} = 0 \tag{25}$$

$$t_{b,\mathrm{id},T}^{\gamma} = TC + R_j^{(1)}(g_{i\,\mathrm{next}}) + \frac{q_j}{s_j}(t_b - \tau_{j,T}) - t_b - \left(\frac{t_{b,\mathrm{acc},T} + t_{b,\mathrm{dec},T}}{2}\right) \tag{26}$$

The cruising time of transit vehicles that stop and do not stop during cycle T is given by Equations 27 and 28, respectively:

$$t_{b,\mathrm{cr},T}^{\alpha/\gamma} = \frac{L_1 + L_2}{v_{b,\mathrm{cr}}} - \frac{t_{b,\mathrm{acc},T} + t_{b,\mathrm{dec},T}}{2} \tag{27}$$

$$t_{b,\mathrm{cr},T}^{\beta} = \frac{L_1 + L_2}{v_{b,\mathrm{cr}}} \tag{28}$$

So that the right equations for a transit vehicle's operating time are considered, three integer variables (ω_b^{α}, ω_b^{β}, ω_b^{γ}), which correspond to time intervals (α, β, γ), are introduced. If the transit vehicle arrives during interval f, ω_b^f will be equal to 1; otherwise, 0 for $f \in \{\alpha, \beta, \gamma\}$.

Hence, the total transit emissions component of the objective function becomes

$$\sum_{b=1}^{B_T}\sum_m e_m^b t_{b,m} = \sum_{b=1}^{B_T}\left[\begin{array}{l} e_{\mathrm{acc}}^b\left[\left(\omega_b^{\alpha}+\omega_b^{\gamma}\right)t_{b,\mathrm{acc},T}\right] + e_{\mathrm{dec}}^b\left[\left(\omega_b^{\alpha}+\omega_b^{\gamma}\right)t_{b,\mathrm{dec},T}\right] \\ +e_{\mathrm{id}}^b\left[\begin{array}{l}\omega_b^{\alpha}\left[\begin{array}{l}(T-1)C + R_j^{(1)}(g_{i,T}) + \frac{q_j}{s_j}(t_b - \tau_{j,T-1}) \\ -t_b - \left(\frac{t_{b,\mathrm{acc},T}+t_{b,\mathrm{dec},T}}{2}\right)\end{array}\right] \\ +\omega_b^{\gamma}\left[\begin{array}{l}TC + R_j^{(1)}(g_{i\,\mathrm{next}}) + \frac{q_j}{s_j}(t_b - \tau_{j,T}) \\ -t_b - \left(\frac{t_{b,\mathrm{acc},T}+t_{b,\mathrm{dec},T}}{2}\right)\end{array}\right]\end{array}\right] \\ +e_{\mathrm{cr}}^b\left[\begin{array}{l}\left(\omega_b^{\alpha}+\omega_b^{\gamma}\right)\left[\left(\frac{L_1+L_2}{v_{b,\mathrm{cr}}}\right) - \left(\frac{t_{b,\mathrm{acc},T}+t_{b,\mathrm{dec},T}}{2}\right)\right] \\ +\omega_b^{\beta}\left(\frac{L_1+L_2}{v_{b,\mathrm{cr}}}\right)\end{array}\right]\end{array}\right] \tag{29}$$

Mathematical Program Formulation

The objective of the proposed optimization problem is to minimize total emissions that can be estimated, as shown in the previous section. This optimization problem is a mixed integer nonlinear program because of the existence of both continuous, $g_{i,T}$, and integer, ω_b^f, variables. As in the case of the person-based mathematical program of Christofa et al. (*24*), the objective function consists of bilinearities because of multiplication of the continuous variables $g_{i,T}$ with the integer variables ω_b^f. The method suggested by Floudas (*28*) and used by Christofa et al. (*24*) is used to address this problem. More details on this method are available in the work of Christofa et al. (*24*). This mixed integer nonlinear program can be solved with the use of the branch and bound method to identify the global minimum as long as the objective function remains convex. For the tests performed in this study, the Hessian matrix of the objective function is positive definite, and so the objective function is convex. For the solution of the subsequent nonlinear programs of each branch, the MATLAB fmincon function is used (*29*). The computation time is on the order of a few seconds, which is sufficient for real-time operations.

TEST SITE

The proposed emission-based signal control system was evaluated with geometric, traffic, and signal timing data from a real-world intersection: Mesogeion and Katechaki Avenues in Athens, Greece. This intersection has high traffic volumes, and nine conflicting transit routes have headways that vary from 15 to 40 min each. Autos and buses share the same lanes. The intersection includes bus stops, which have been ignored for this study. Figure 3 illustrates the intersection's layout. The volume data have been obtained from detectors located 40 m upstream of the intersection for 7:00 to 8:00 a.m. The intersection operates on a six-phase cycle and has a flow ratio of $Y = 0.9$

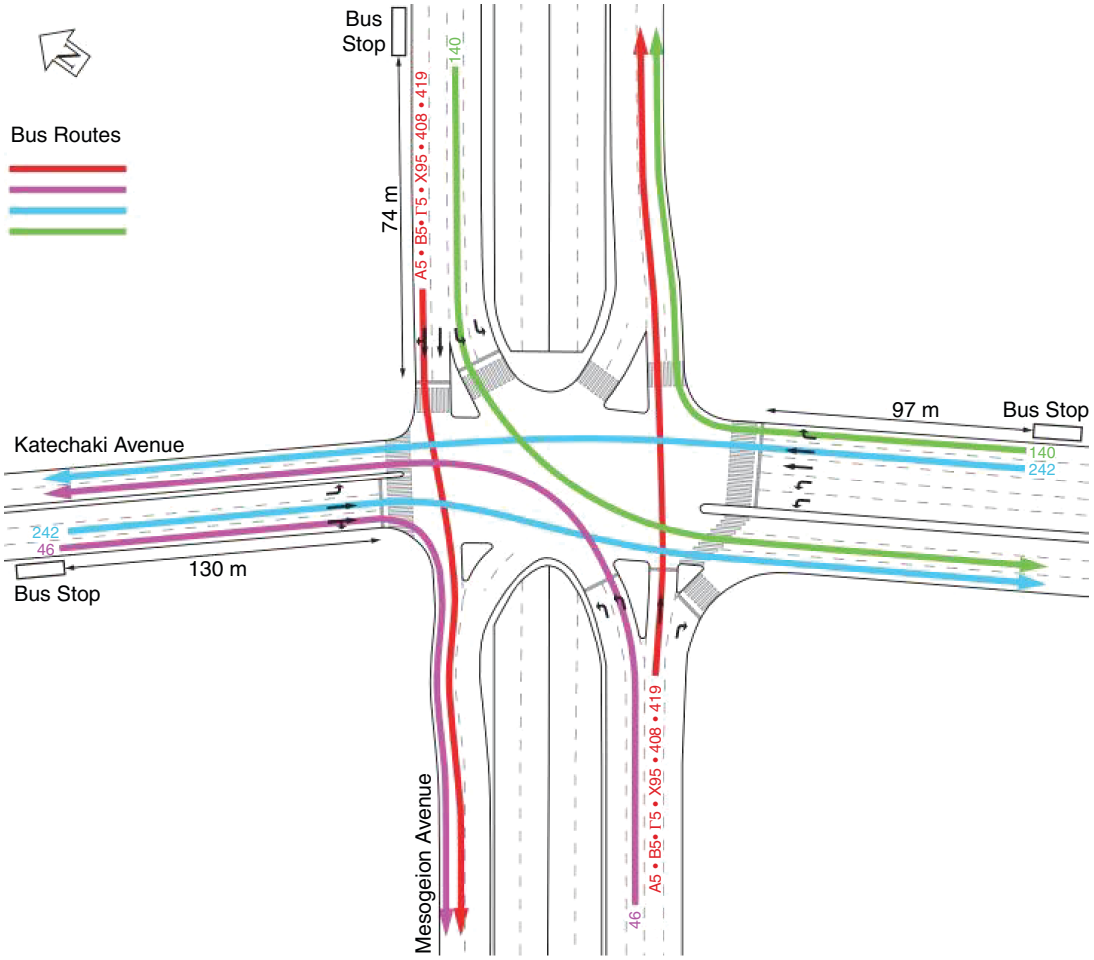

FIGURE 3 Layout and bus routes for intersection of Mesogeion and Katechaki Avenues (*24*).

during this period. Intersection flow ratio is the sum of flow ratios (the ratio of demand to saturation flow) for each critical lane group per signal phase at the intersection (*26*). An intersection flow ratio of 0.9 implies close to saturated conditions, where cycle length $C = 120$ s and lost time $L = 14$ s. Information about bus schedules was obtained from the Athens Urban Transport Organisation website (*30*).

EVALUATION

Two types of tests are performed to evaluate the performance of the emission-based signal timing optimization: (*a*) deterministic arrival tests and (*b*) stochastic arrival tests. Deterministic arrival tests are performed under the assumption that perfect information about transit vehicle arrival times, auto flows and arrival times, and auto and transit vehicle passenger occupancy is available in real time and without errors. In addition, the automobile arrival flows at every lane group are assumed to be constant across all cycles. Deterministic arrival tests also assume constant acceleration and deceleration rates. Stochastic arrival tests are performed with the microsimulation software AIMSUN (*31*) and emulation-in-the-loop simulation (EILS). EILS utilizes the advanced programming interface of AIMSUN to model the proposed emission-based traffic control system as well as the previously published person-based signal timing optimization algorithm. This way, the real-time signal control systems can be tested in an environment closer to the real world, where there is stochasticity in auto arrival flows and times as well as in transit vehicle arrival times. In particular, the prediction of auto arrivals was based on detectors located approximately 40 m upstream from the intersection and a second set of detectors located at the exit of each lane group. Exponential smoothing was used on the measured flows of both sets of detectors during the previous cycle to predict auto arrival flows. Prediction of transit vehicle arrival times was based on information collected by detectors located upstream on entry links at distances from the intersection equivalent to the travel time of one cycle length. This way, a transit vehicle's arrival at the intersection could be known one cycle in advance. A more detailed description of the auto and transit vehicles' arrival estimation for the stochastic arrival tests is available elsewhere (*24*).

As mentioned, $g_{i\,\mathrm{next}}$ is a user-specified value for the green time of the next cycle, which is used to estimate the delay and emissions of the next cycle. The value of $g_{i\,\mathrm{next}}$ is set to the initial value of the fixed optimized green times obtained by TRANSYT-7F (*27*). Green times of each phase were constrained by maximum and minimum green times, $g_{i\,\max}$ and $g_{i\,\min}$; $g_{i\,\max}$ is set to $C - \sum_{i=1}^{I} y_i$, and $g_{i\,\min}$ is set to 7 s for left-turning movements and to 10 s for through movements. These inputs were consistent between the two types of tests.

TABLE 1 Modal Emission Rates

Vehicle Type	Operating Mode	NO_x (mg/s)	HC (mg/s)
Gasoline autos	Acceleration	7.7	2.5
	Deceleration	0.9	0.5
	Cruising	1.2	0.4
	Idling	0.3	0.4
Diesel buses	Acceleration	263.5	2.1
	Deceleration	45.0	1.3
	Cruising	133.3	1.7
	Idling	45.0	1.3

NOTE: NO_x = nitrogen oxide; HC = hydrocarbon.

The normal acceleration and deceleration rates of automobiles at urban intersections were considered to be 3 m/s^2 and 4 m/s^2, respectively. Transit vehicles were assumed to have the same rate for both acceleration and deceleration, which is equal to 2 m/s^2. An average cruising speed of 45 km/h was considered for both auto and transit vehicles. Finally, the upstream and downstream distances, L_1 and L_2, used to ensure that vehicles were completing a full operating cycle were set to 150 and 80 m, respectively.

The emission rates used in this study were calculated for the VSP mode for both autos and buses. The focus was on gasoline autos and diesel buses. As previous studies have illustrated, the level of a vehicle's specific power is a function of its link's grade, as well as its speed and acceleration rate (*20*). The assignment of the proper VSP bin to every vehicle operating mode is done under the assumption that the link grade is zero. More specifically, for every second of a vehicle that is accelerating, VSP was estimated with the constant acceleration rate assumed and the average value of the speed of that time interval. Then, the emission rate for each VSP mode was estimated for two pollutants, hydrocarbon (HC) and nitrogen oxide (NO_x), according to rates provided by Frey et al. (*20*) for gasoline autos and Zhai et al. (*21*) for diesel buses. Finally, for calculating emission rates per time spent in acceleration, deceleration, idling, and cruising modes separately, the emission rates of the VSP bins included in these modes were averaged. Table 1 shows the emission rates per operating mode that were used for gasoline autos and diesel buses.

Three scenarios were tested for each of the two types of tests: (*a*) vehicle-based, (*b*) person-based, and (*c*) emission-based optimization; the results of these were compared. To account for variations in bus arrival times, each scenario was tested 20 times for both deterministic and stochastic arrival tests. Six tests were conducted with varying intersection flow ratios, *Y,* from 0.4 to 0.9; $Y = 0.4$ corresponds to a very low level of saturation, and $Y = 0.9$ corresponds to nearly saturated conditions. An average occupancy of $\overline{o}_a = 1.25$ passengers per vehicle was considered for all autos, and an average occupancy of $\overline{o}_a = 40$ passengers per vehicle was considered for all transit vehicles. In the deterministic arrival tests, that value was based on the schedule delay of the bus. The higher the difference between a bus arrival time at the intersection and its scheduled arrival time, the higher the number of passengers it was carrying. For the stochastic arrival tests, a random passenger occupancy was given to each transit vehicle, with an average value of 40 passengers per vehicle.

RESULTS

Figure 4, *a* and *b,* illustrates the improvement in HC emissions from vehicle-based and person-based scenarios, respectively, to the emission-based scenario for the deterministic arrival tests. The figure shows that total HC emissions can be reduced on average by up to 2.5% and 4.4% compared with vehicle-based and person-based total HC emission levels, respectively. The lower the intersection flow ratio, the higher the total emission reduction achieved. This occurs because at lower intersection flow ratios there is more flexibility in the cycle for adjustment of green times to achieve substantial reduction in emissions. Figure 4*a* also indicates that most of the emission reduction is attributable to reduced bus emissions, because of buses' higher emission rates for deceleration, cruising, and idling compared with autos. This implies that buses are stopped fewer times. Hence, some level of transit signal priority can be provided through emission-based optimization for

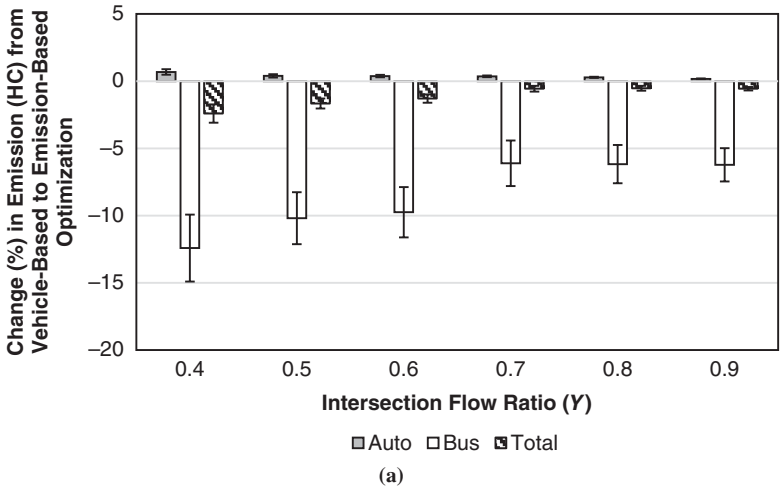

FIGURE 4 Percentage of change in HC emissions for HC emission–based optimization for various intersection flow ratios and $\overline{o}_a/\overline{o}_b$ = 40/1.25: (*a*) from vehicle-based to HC emission–based optimization (deterministic arrival tests).

(continued on next page)

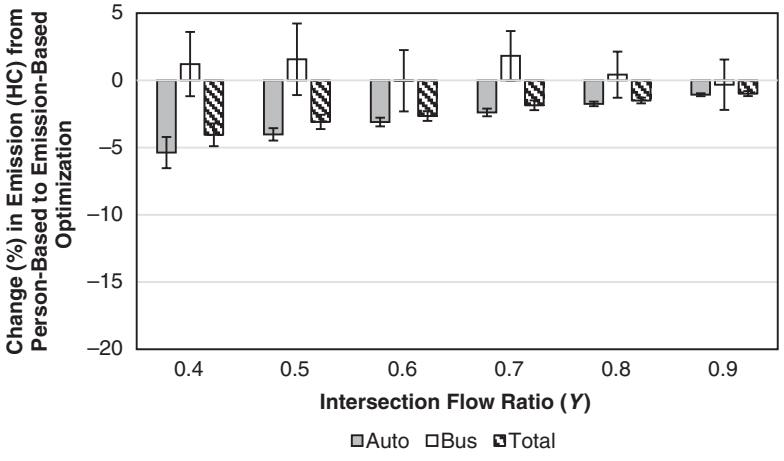

(b)

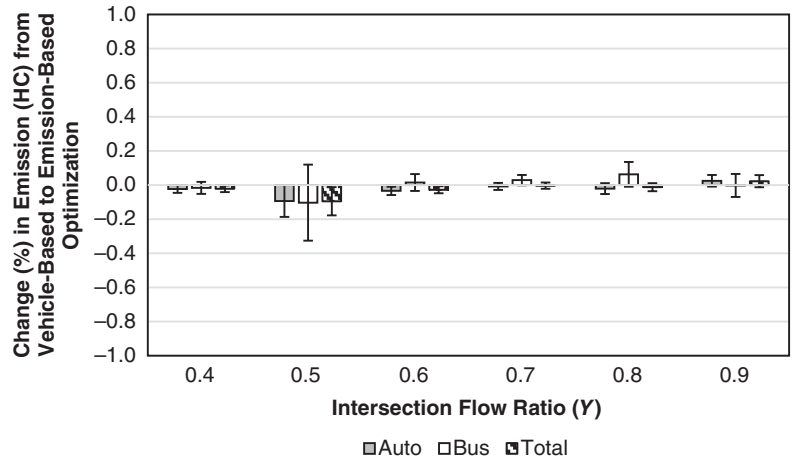

(c)

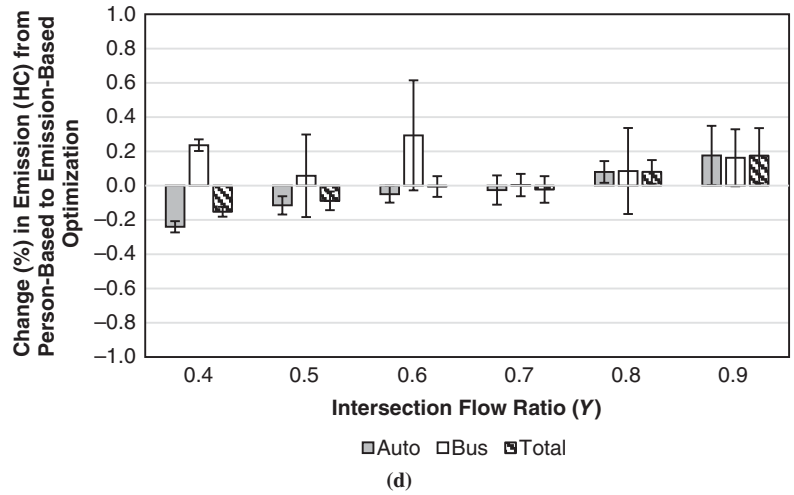

(d)

FIGURE 4 *(continued)* Percentage of change in HC emissions for HC emission–based optimization for various intersection flow ratios and $\bar{o}_a/\bar{o}_b$ = 40/1.25: (*b*) from person-based to HC emission–based optimization (deterministic arrival tests), (*c*) from vehicle-based to HC emission–based optimization (stochastic arrival tests), and (*d*) from person-based to HC emission–based optimization (stochastic arrival tests).

HC compared with vehicle-based optimization. A comparison of person-based optimization and emission-based optimization indicates that the change in bus emissions is negligible, but an average reduction in auto emissions by up to 5.4% is observed (Figure 4*b*).

The stochastic arrival test results for the same scenarios are shown in Figure 4, *c* and *d.* Because of the lack of perfect information in the simulation tests and the need to predict vehicle arrivals, the percentage changes for both comparisons (vehicle-based to emission-based and person-based to emission-based) reveal results that are not statistically significant as implied by the 95% confidence intervals shown in the graphs. Only for very light traffic conditions ($Y = 0.4$) does a comparison of the person-based and emission-based scenarios show some benefits for overall emissions but increasing bus emissions.

At the same time, total person delay decreases by up to 15% and bus person delay by up to 33% for low intersection flow ratios and deterministic arrival tests on average (Figure 5*a*). Compared with person-based optimization, bus person delay can increase on average by up to 41% (Figure 5*b*), indicating the higher effectiveness of person-based optimization for providing priority to buses and reducing their delay, compared with emission-based optimization. However, total person delay experiences only minor changes. Stochastic arrival tests reveal similar results but present no statistically significant percentage change differences for high intersection flow ratios (Figure 5*c*) and lower bus person delay increases (Figure 5*d*) compared with the deterministic arrival test results.

Deterministic arrival tests that minimize NO_x emissions demonstrate improvements in total emissions from 3.6% to 6.7% and bus emissions from 4.6% to 7.6% on average, depending on the intersection flow ratio when vehicle-based and emission-based optimization are compared (Figure 6*a*). For stochastic arrival tests, emission-based optimization appears to be effective for minimizing total emissions for intersection flow ratios up to 0.5 (Figure 6*c*). As before, stochasticity in arrivals affects the accuracy of auto and bus arrival predictions, and the inaccuracies are higher at more congested traffic conditions. In a comparison of person-based and

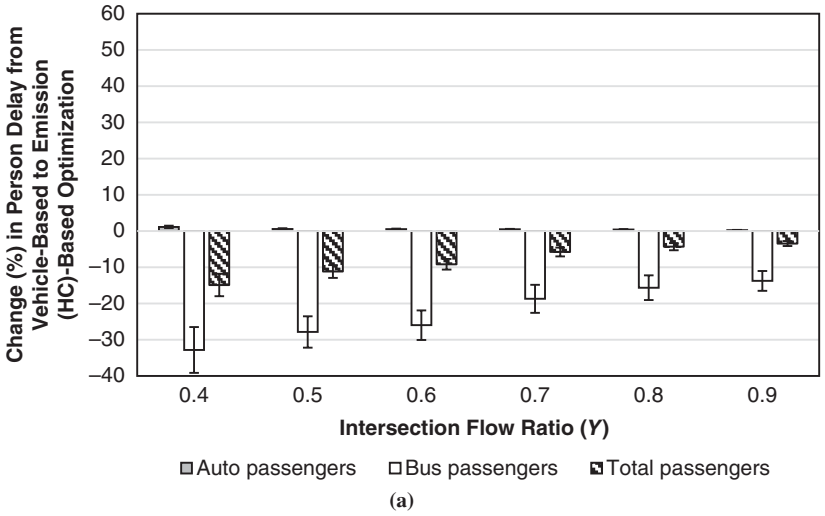

FIGURE 5 Percentage of change in person delay for HC emission–based optimization for various intersection flow ratios and $\bar{o}_a/\bar{o}_b$ = 40/1.25: (*a*) from vehicle-based to HC emission–based optimization (deterministic arrival tests) and (*b*) from person-based to HC emission–based optimization (deterministic arrival tests).

(continued on next page)

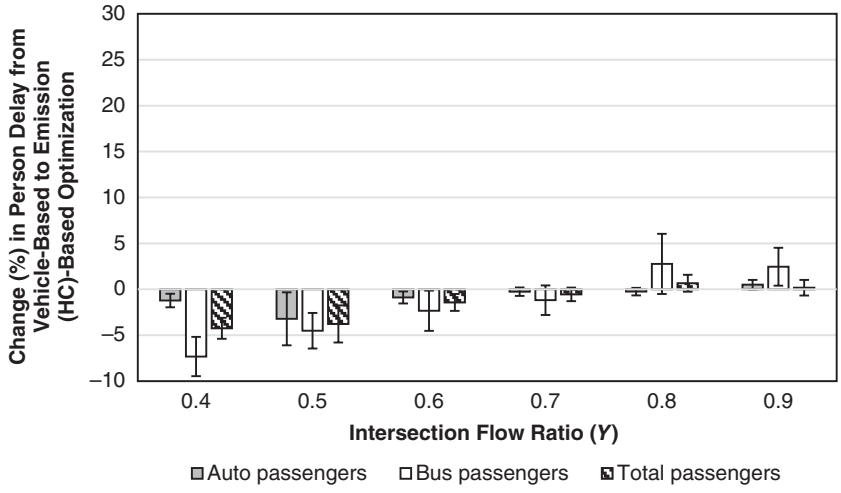

(c)

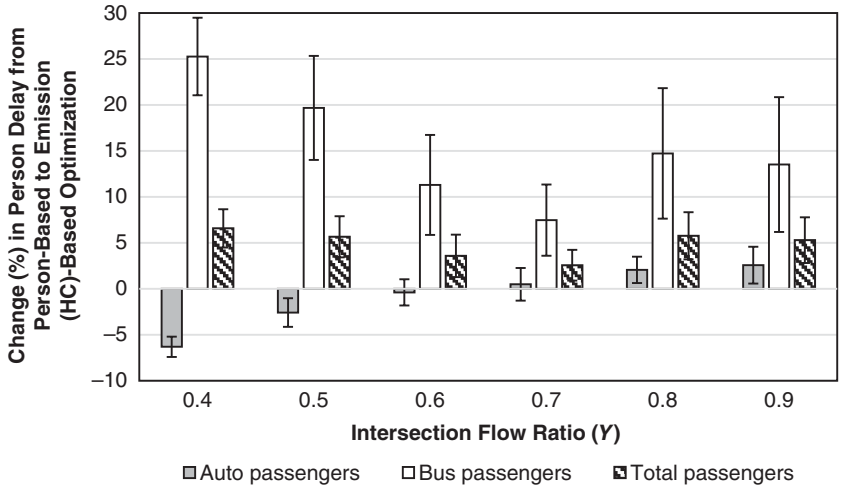

(d)

FIGURE 5 *(continued)* Percentage of change in person delay for HC emission–based optimization for various intersection flow ratios and $\bar{o}_a/\bar{o}_b$ = 40/1.25: (*c*) from vehicle-based to HC emission–based optimization (stochastic arrival tests) and (*d*) from person-based to HC emission–based optimization (stochastic arrival tests).

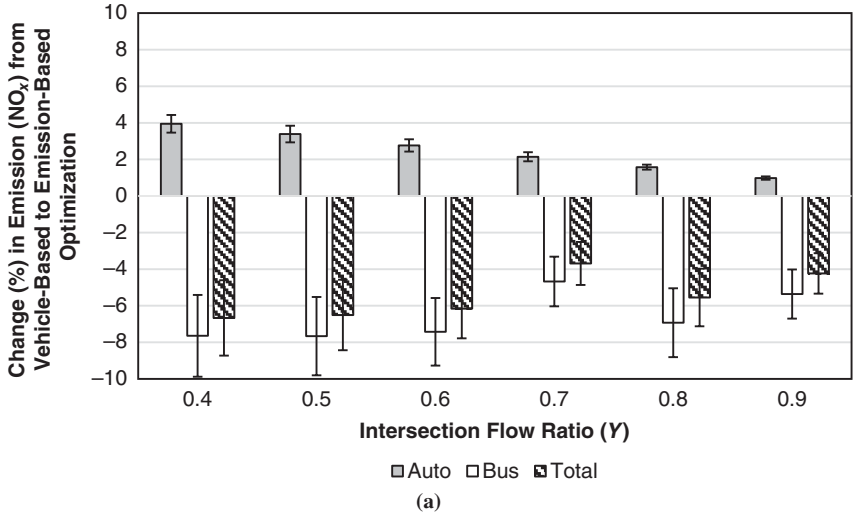

(a)

FIGURE 6 Percentage of change in NO_x emissions for NO_x emission–based optimization for various intersection flow ratios and $\bar{o}_a/\bar{o}_b$ = 40/1.25: (*a*) from vehicle-based to NO_x emission–based optimization (deterministic arrival tests).

(continued)

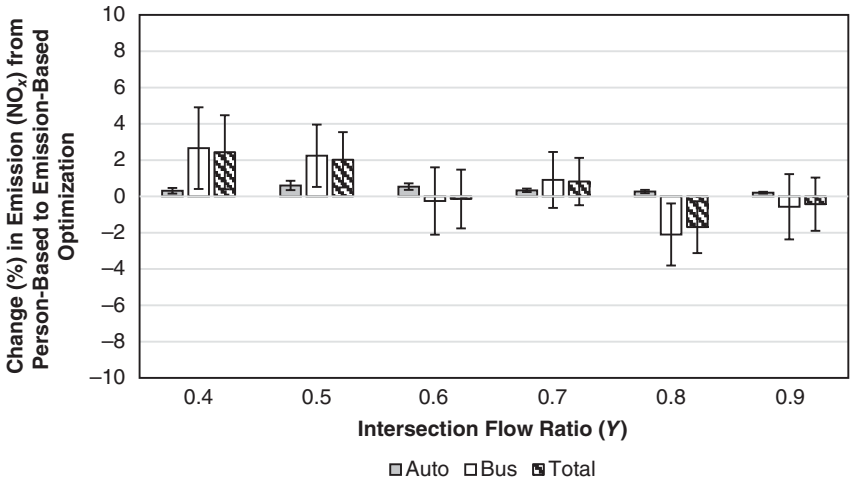

(b)

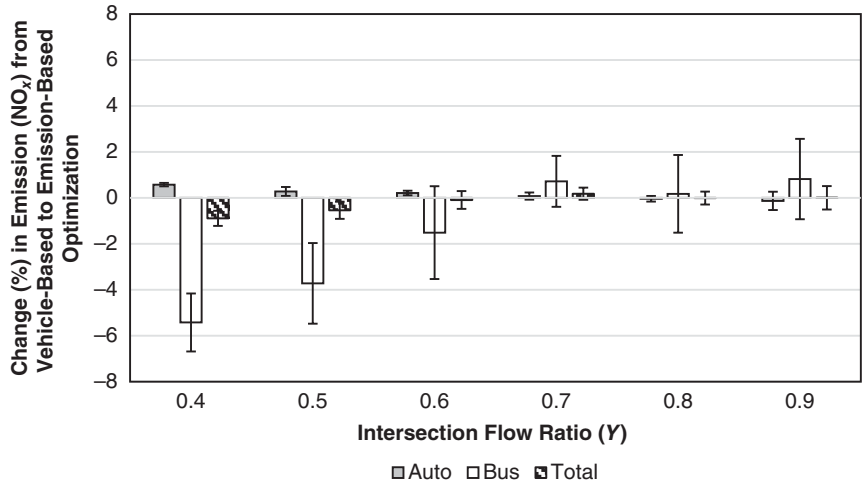

(c)

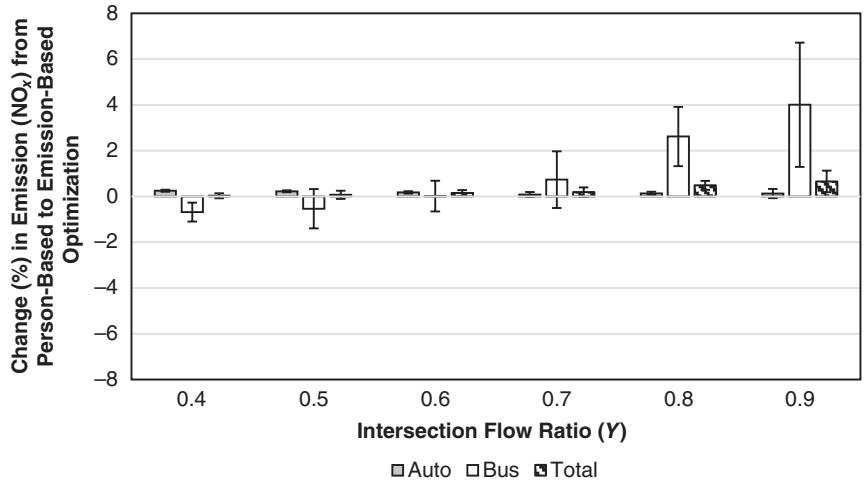

(d)

FIGURE 6 *(continued)* Percentage of change in NO_x emissions for NO_x emission–based optimization for various intersection flow ratios and $\bar{o}_a/\bar{o}_b$ = 40/1.25: (*b*) from person-based to NO_x emission–based optimization (deterministic arrival tests), (*c*) from vehicle-based to NO_x emission–based optimization (stochastic arrival tests), and (*d*) from person-based to NO_x emission–based optimization (stochastic arrival tests).

NO_x emission–based optimization, the differences in the results are not statistically significant (Figure 6, *b* and *d*), and for some intersection flow ratios in the stochastic arrival tests results are not consistent (Figure 6*d*).

A comparison of person delay from vehicle-based and NO_x emission–based optimization shows reductions in total person delay of up to 15% and bus person delay of up to 47% on average for deterministic arrival tests (Figure 7*a*) and lower percentage of changes on average of up to about 11% and 29%, respectively, for stochastic arrival tests (Figure 7*c*). A comparison of person-based optimization with NO_x emission–based optimization reveals statistically significant differences in person delays for only low intersection flow ratios (Figure 7, *b* and *d*).

A comparison of the results for the NO_x emission–based and HC emission–based optimization scenarios shows that higher emission reductions are achieved with the former because the emission rates for each operating mode for NO_x are higher than those for HC.

CONCLUSION

This paper presented a real-time signal control system that minimizes total auto and transit vehicle emissions at an isolated intersection in undersaturated traffic conditions. The results of the evaluation of the proposed system, using data from a real-world intersection in Athens, Greece, indicate that the proposed system can reduce both total emissions and person delay, compared with a vehicle-based optimization scenario. Additionally, transit person delay in the proposed scenario is considerably reduced, which could improve transit ridership. The evaluation results also show that it can reduce total emissions compared with the person-based optimization system. A sensitivity analysis with respect to intersection flow ratio shows that the developed system is more effective in reducing total emissions and person delay for lower intersection flow ratios. As the flow ratio increases, the vehicle-based and emission-based signal optimization systems converge because the higher auto demand at nearly saturated conditions

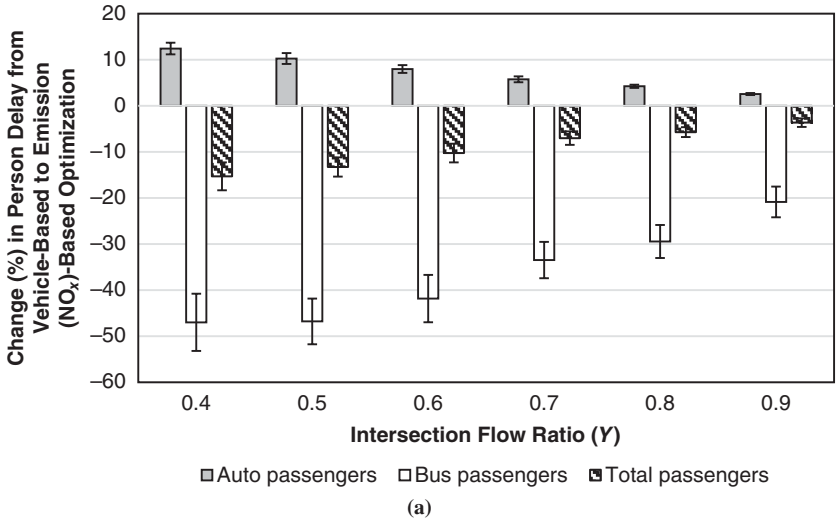

(a)

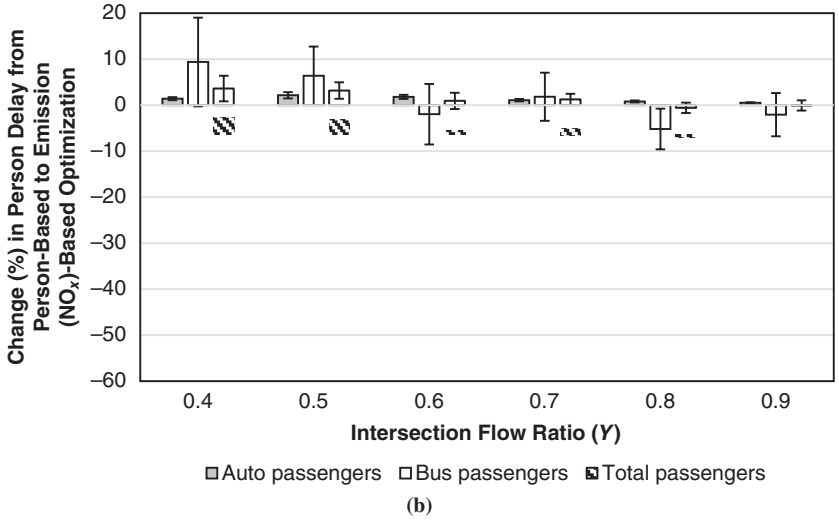

(b)

FIGURE 7 Percentage of change in person delay for NO_x emission–based optimization for various intersection flow ratios and $\bar{o}_a/\bar{o}_b$ = 40/1.25: (*a*) from vehicle-based to NO_x emission–based optimization (deterministic arrival tests) and (*b*) from person-based to NO_x emission–based optimization (deterministic arrival tests).

(continued)

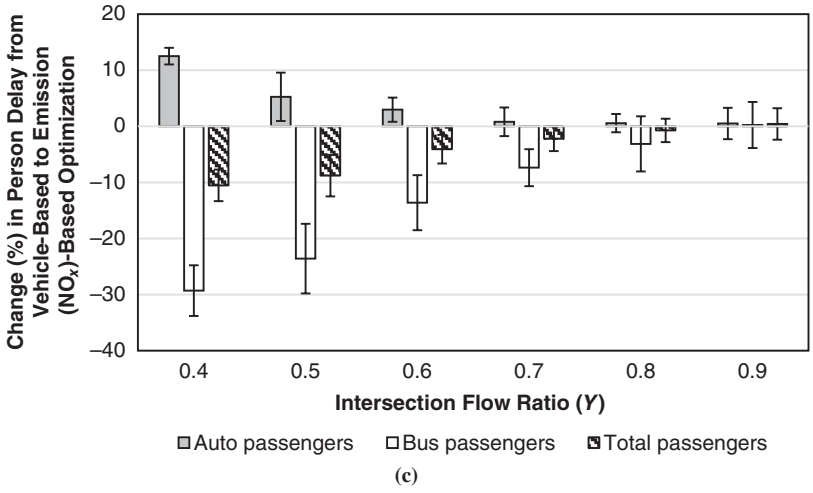

(c)

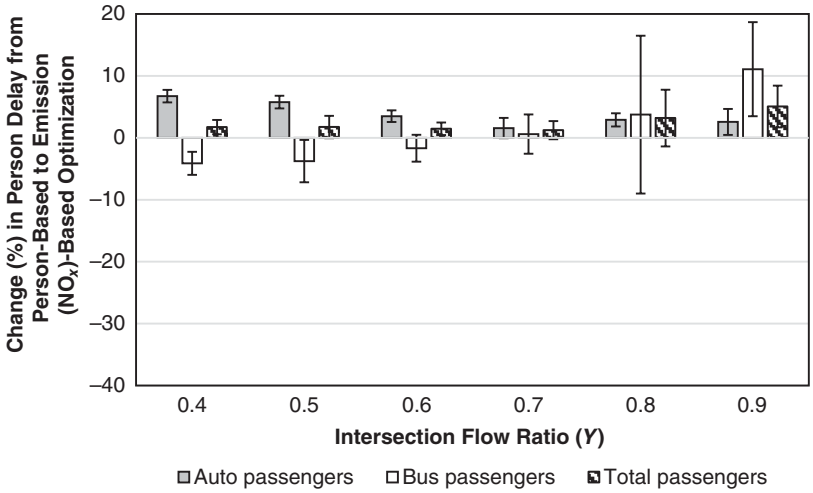

(d)

FIGURE 7 *(continued)* Percentage of change in person delay for NO_x emission–based optimization for various intersection flow ratios and $\bar{o}_a/\bar{o}_b$ = 40/1.25: (*c*) from vehicle-based to NO_x emission–based optimization (stochastic arrival tests) and (*d*) from person-based to NO_x emission–based optimization (stochastic arrival tests).

outweighs the weight given to transit vehicles because of their higher emission potential. In addition, stochastic arrival tests indicated that the loss in accuracy of auto and transit vehicle arrivals occurring in a more realistic environment causes deteriorating performance of the emission- and person-based optimization methods, especially for traffic conditions close to saturation.

This study has shown that both the proposed emission-based optimization and the person-based optimization previously developed can be used to provide priority to transit vehicles and reduce overall emissions at intersections, compared with commonly used vehicle-based optimization methods. The study also verified that person-based optimization is still the preferred method for improving person mobility, and emission-based optimization should be used when the primary focus is on improving air quality at intersections. The results are sensitive to the specific emission rates used, are expected to differ by vehicle type, and will depend on a mix of these. In addition, although the presented results are for certain pollutants, that is, HC and NO_x, the same method could be implemented with emission rates per operating mode for any other pollutant. Future work will include extending the emission-based optimization system to a signalized corridor and oversaturated traffic conditions.

ACKNOWLEDGMENT

This research was sponsored by the U.S. Department of Transportation through the New England University Transportation Center.

REFERENCES

1. Hall, J. V. Assessing Health Effects of Air Pollution. *Atmospheric Environment,* Vol. 30, No. 5, 1996, pp. 743–746.
2. Hunt, P., D. Robertson, R. Bretherton, and M. Royle. The SCOOT On-Line Traffic Signal Optimization Technique. *Traffic Engineering and Control,* Vol. 23, No. 4, 1982, pp. 190–192.
3. Sen, S., and K. L. Head. Controlled Optimization of Phases at an Intersection. *Transportation Science,* Vol. 31, No. 1, 1997, pp. 5–17.
4. Zhang, Y., X. Chen, X. Zhang, G. Song, Y. Hao, and L. Yu. Assessing Effect of Traffic Signal Control Strategies on Vehicle Emissions. *Journal*

of Transportation Systems Engineering and Information Technology, Vol. 9, No. 1, 2009, pp. 150–155.
5. Zhang, L., Y. Yin, and S. Chen. Robust Signal Timing Optimization with Environmental Concerns. *Transportation Research Part C: Emerging Technologies,* Vol. 29, 2013, pp. 55–71.
6. Yagar, S., B. Han, and J. Greenough. Real-Time Signal Control for Mixed Traffic and Transit Based on Priority Rules. In *Traffic Management: Proceedings of the Engineering Foundation Conference,* 1992.
7. Wang, Y., D. Guo, S. Li, Y. Wang, and Z. Li. Signal Timing Optimization Simulation on Urban Road Intersection based on Vehicle Emissions. *Proc., 8th International Conference of Chinese Logistics and Transportation Professionals Logistics,* 2008, pp. 4762–4767.
8. Frey, H.C., N.M. Rouphail, A. Unal, and J. Colyar. *Emissions Reduction Through Better Traffic Management: An Empirical Evaluation Based Upon On-Road Measurements.* Technical Report FHWY/NC/2002-001. North Carolina Department of Transportation, Raleigh, 2001.
9. Rouphail, N.M., H.C. Frey, J.D. Colyar, and A. Unal. Vehicle Emissions and Traffic Measures: Exploratory Analysis of Field Observations at Signalized Arterials. Presented at 80th Annual Meeting of the Transportation Research Board, Washington, D.C., 2001.
10. Unal, A., N.M. Rouphail, and H.C. Frey. Effect of Arterial Signalization and Level of Service on Measured Vehicle Emissions. In *Transportation Research Record: Journal of the Transportation Research Board, No. 1842,* Transportation Research Board of the National Academies, Washington, D.C., 2003, pp. 47–56.
11. Chen, K., and L. Yu. Microscopic Traffic-Emission Simulation and Case Study for Evaluation of Traffic Control Strategies. *Journal of Transportation Systems Engineering and Information Technology,* Vol. 7, No. 1, 2007, pp. 93–99.
12. Horiguchi, R., M. Katakura, H. Akahane, and M. Kuwahara. A Development of a Traffic Simulator for Urban Road Networks: AVENUE. *Proc., IEEE Vehicle Navigation and Information Systems Conference,* 1994, pp. 245–250.
13. Stevanovic, A., J. Stevanovic, K. Zhang, and S. Batterman. Optimizing Traffic Control to Reduce Fuel Consumption and Vehicular Emissions: Integrated Approach with VISSIM, CMEM, and VISGAOST. In *Transportation Research Record: Journal of the Transportation Research Board, No. 2128,* Transportation Research Board of the National Academies, Washington, D.C., 2009, pp. 105–113.
14. Rakha, H., and K. Ahn. Integration Modeling Framework for Estimating Mobile Source Emissions. *Journal of Transportation Engineering,* Vol. 130, No. 2, 2004, pp. 183–193.
15. Madireddy, M.R., B. De Coensel, I. De Vlieger, D. Botteldooren, B. Beusen, B. Degrauwe, G. Lenaers, A. Can, and A. Eijk. Microsimulation of a Traffic Fleet to Predict the Impact of Traffic Management on Exhaust Emissions. *Proc., 18th International Symposium on Transport and Air Pollution,* EMPA, Dübendorf, Switzerland, 2010.
16. Shabihkhani, R., and E.J. Gonzales. Analytical Model for Vehicle Emissions at Signalized Intersection: Integrating Traffic and Microscopic Emissions Models. Presented at 92nd Annual Meeting of the Transportation Research Board, Washington, D.C., 2013.
17. Skabardonis, A., N. Geroliminis, and E. Christofa. Prediction of Vehicle Activity for Emissions Estimation Under Oversaturated Conditions Along Signalized Arterials. *Journal of Intelligent Transportation Systems,* Vol. 17, No. 3, 2013, pp. 191–199.
18. Song, G., L. Yu, and Y. Zhang. Applicability of Traffic Microsimulation Models in Vehicle Emissions Estimates: Case Study of VISSIM. In *Transportation Research Record: Journal of the Transportation Research Board, No. 2270,* Transportation Research Board of the National Academies, Washington, D.C., 2012, pp. 132–141.
19. Rakha, H., and Y. Ding. Impact of Stops on Vehicle Fuel Consumption and Emissions. *Journal of Transportation Engineering,* Vol. 129, No. 1, 2003, pp. 23–32.
20. Frey, H.C., N.M. Rouphail, and H. Zhai. Speed- and Facility-Specific Emission Estimates for On-Road Light-Duty Vehicles on the Basis of Real-World Speed Profiles. In *Transportation Research Record: Journal of the Transportation Research Board, No. 1987,* Transportation Research Board of the National Academies, Washington, D.C., 2006, pp. 128–137.
21. Zhai, H., H.C. Frey, and N.M. Rouphail. A Vehicle-Specific Power Approach to Speed and Facility-Specific Emissions Estimates for Diesel Transit Buses. *Environmental Science and Technology,* Vol. 42, No. 21, 2008, pp. 7985–7991.
22. Barth, M., F. An, T. Younglove, C. Levine, G. Scora, M. Ross, and T. Wenzel. *NCHRP Project 25-11: Development of a Comprehensive Modal Emissions Model.* TRB, National Research Council, Washington, D.C., 2000.
23. Christofa, E., and A. Skabardonis. Traffic Signal Optimization with Application of Transit Signal Priority to an Isolated Intersection. In *Transportation Research Record: Journal of the Transportation Research Board, No. 2259,* Transportation Research Board of the National Academies, Washington, D.C., 2011, pp. 192–201.
24. Christofa, E., I. Papamichail, and A. Skabardonis. Person-Based Traffic Responsive Signal Control Optimization. *IEEE Transactions on Intelligent Transportation Systems,* Vol. 14, No. 3, 2013, pp. 1278–1289.
25. Coelho, M.C., H.C. Frey, N.M. Rouphail, H. Zhai, and L. Pelkmans. Assessing Methods for Comparing Emissions from Gasoline and Diesel Light-Duty Vehicles Based on Microscale Measurements. *Transportation Research Part D: Transport and Environment,* Vol. 14, No. 2, 2009, pp. 91–99.
26. *Highway Capacity Manual.* TRB, National Research Council, Washington, D.C., 2000.
27. Wallace, C., K. Courage, M. Hadi, and A. Gan. *TRANSYT-7F User's Guide.* University of Florida, Gainesville, 1998.
28. Floudas, C.A. *Nonlinear and Mixed-Integer Optimization: Fundamentals and Applications.* Oxford University Press, Oxford, United Kingdom, 1995.
29. *MATLAB User's Manual.* The MathWorks, Natick, Mass., 2009.
30. *Search Routes.* Athens Urban Transport Organisation, 2010. http://www.oasa.gr.
31. *Aimsun Users Manual Version 8.* Transport Simulation Systems, Barcelona, Spain, 2014.

The Standing Committee on Traffic Signal Systems peer-reviewed this paper.